Check for updates

ChemistrySelect

Research Article
doi.org/10.1002/slct.202402216

Chemistry Europe
European Chemical Societies Publishing

www.chemistryselect.org

Synthesis and Property Evaluations of a Bio-Based Anticorrosive Urethane Composites Containing Bisphenol a as Extender

Samuel Adeboye,[a] Adedamola Adebowale,[a] Bamidele Durodola,[a] Bolatito Olanipekun,[b] Kolawole Ajanaku,[a] Emmanuel Akintayo,[c] Pratyay Basak,[d] Ramanuj Narayan,[d] and Tolutope Siyanbola*[a, d]

This article reports the synthesis of an eco-friendly polyurethane composite system, which was successfully prepared in a one-pot synthetic pathway by combining castor seed oil (CSO), bisphenol A (BPA), isophorone diisocyanate (IPDI), and functional hybrid nanoparticles (prepared by modifying the peripheral surface of silica with 3-aminopropyltrimethoxysilane (APTMS). The urethane composites were cast as thin films on tin foils and mild steel and cured under atmospheric moisture. Attenuated total reflectance Fourier transform infrared (ATR-FTIR) spectroscopy was used to characterise the cured composite films, scanning electron microscopy (SEM), energy dispersive X-ray (EDX), X-ray diffraction (XRD), thermogravimetric analysis (TGA), corrosion resistance, antimicrobial analysis, salt spray test, and water contact angle measurements. Our evaluations showed improved thermal and hydrophobic properties of the composite coatings. Also, the electrochemical and antimicrobial analyses clearly show resistance to corrosion and test organisms as the percentage composition of APTMS-SiO_2 increases in the urethane system.

1. Introduction

The onset of coating development focused on the aesthetics and protection the covering would provide on various substrates. The evolution of functional coatings has brought to the limelight the use of nanoparticles, fillers, and other materials to improve synthesised coating systems' electrical, chemical, physical, optical, and mechanical properties.[1,2] Nanoparticles and their hybrid forms have also been shown to enhance fire retardancy, corrosion resistance, self-cleaning, self-healing, anti-fouling, and antimicrobial properties.[3,4] The high surface area to volume ratio of nanoparticles is responsible for these enhancing properties in urethane systems. Nanosized inorganic metal oxides like MgO, ZrO_2, ZnO, Al_2O_3, Fe_2O_3, CeO_2, TiO_2, and SiO_2 have been used directly and in modified forms in several coating composite formulations.[5–11] Silica nanoparticles (Si-NPs) are prognostic materials used widely in biomedical applications such as imaging,[12,13] drug delivery,[14] therapeutic drug monitoring,[15] sensing,[16] and catalysis.[17] Notably, SiO_2-based materials play a role the development of biometric superhydrophobic surfaces.[18] The United States Food and Drug Administration's (FDA) recognition of silica as a safe material, and the growing interest in this multifunctional material due to its biocompatibility, degradability, versatile siloxane chemistry, and chemical inertness are reasons why researchers have a keen interest in the study and applications of SiNPs.[19,20] SiNPs can be obtained via hydrothermal, mechanochemical, wet chemical, and most prominently sol-gel methods.[21,22] Surface modification is commonly accomplished by performing silylation processes that specifically target the exposed surface silanols.[23] Additional methods involve the simultaneous condensation with organoalkoxysilanes in a single-step sol-gel synthesis and the application of surface polymerisation to repair polymer coatings.[24] This study examines the contributions of modified silica (SiO_2) blended with bisphenol A in a one-pot polyurethane coating system. The 3-aminopropyltrimethoxysilane (APTMS) modified silica (APTMS-SiO_2) stabilizes in the urethane polymer matrix due to its hybrid nature thereby preventing agglomeration of the particles.[25] The study harnessed the positive contributions of ricinoleic fatty acid in castor seed oil (*Ricinus communis*) in the preparation of our coating system. This eco-friendly and sustainable seed oil provides the reactive hydroxyl functional group in the urethanation reaction. Plant seed oils of safflower, sunflower, *Pongamia glabra*, soya bean, yellow oleander, Nahar, linseed, etc are usually modified (via transesterification, hydroformylation, epoxidation, aminolysis, partial glyceride (PG) formation etc.) to create a reactive site from the double bonds or cleavage of the triglyceride ester bond.[6,26,27] The prepared modified nanoparticles of SiO_2, films and mild steel-coated panels were

[a] S. Adeboye, A. Adebowale, B. Durodola, K. Ajanaku, T. Siyanbola
Department of Chemistry, Covenant University, P.M.B. 1023, Ota, Ogun State, Nigeria
+2348051156222
E-mail: tolu.siyanbola@covenantuniversity.edu.ng
siyanbola@csiriict.in

[b] B. Olanipekun
Department of Chemistry & Industrial Chemistry, Kwara State University, Malete, Kwara State, Nigeria

[c] E. Akintayo
Department of Chemistry, Ekiti State University, P.M.B. 5363, Ado-Ekiti, Ekiti state, Nigeria

[d] P. Basak, R. Narayan, T. Siyanbola
Polymers and Functional Materials Division, Indian Institute of Chemical Technology, Hyderabad, Telangana State 500 007, India

© 2024 Wiley-VCH GmbH

characterized using attenuated total reflectance Fourier transform infrared (ATR-FTIR) spectroscopy, scanning electron microscopy (SEM), thermogravimetric analysis (TGA), water contact angle, anticorrosive properties (Tafel plots), and antimicrobial properties.

Experimental

Material and Method

Isophorone diisocyanates (IPDI) were obtained from Surechem products, Suffolk, England, Bisphenol A (BPA) 97% was supplied by Sigma Aldrich, USA, 4-methyl-2-pentanone [Methyl Isobuthy Ketone (MIBK)] 99% was supplied by Sigma Aldrich, USA, 3-aminopropyltrimethoxysilane (APTMS), and silica nanopowder (50–70 μm) (SiO_2) were purchased from Sigma-Aldrich, Germany. While Ethanol 98%) and acetone 99.99% (HPLC grade) were obtained from Fisher Scientific, UK), and 98% was purchased from Merck, Germany). Circular and rectangular Teflon mould dishes were purchased from Amazon, India.

Extraction of Oil

Castor seeds were collected from Ado Ekiti, in Ekiti State, Southwestern Nigeria, and dried in the sun to a constant weight. The seeds were cleaned by separating immature and extraneous matter from the lots. This was followed by removing the mesocarp and outermost layer of the seeds. They cracked, and winnowing separated the kennel (fleshy part) from the husk (chaff). The kennels were then stored in a desiccator and ground into a powder using an electric blender. The oil was extracted using a Soxhlet extractor with n-hexane as the solvent.[28]

Preparation of APTMS-Modified SiO_2

Toluene (50 g toluene and 10 g SiO_2 powder was added to a 500 ml round bottom flask and agitated for 10 min with a magnetic stirrer. A 30-minute ultrasonic bath was used to achieve a consistent suspension. Subsequently, 1 g of APTMS was introduced into the suspension and subjected to continuous stirring at ambient temperature for 60 minutes. A pale yellowish transparent colouration was observed. The mixture was then refluxed for 24 hours. The solvent was removed from the APTMS-modified SiO_2 (APTMS-SiO_2) using a rotary evaporator, while excess unreacted APTMS was eliminated by washing with ethanol. The powder was then dried in an oven at 50 °*C* for one hour. The modified powder was then ground and dried at 100 °*C* for 2 hours.[1]

Synthesis of Polyurethane (PU)

A mixture of 5 g of CSO, bisphenol A (BPA) (0.25 g), and the calculated number of APTMS-modified SiO_2 nanoparticles in varying proportions was carefully added to 10 ml of MIBK. The solution was sonicated at 50 °*C* for an hour. A dropping funnel, thermometer, and nitrogen gas inlet were attached to a 250 ml round bottom three-neck flask. 3.00 g) was dissolved in 5 ml of MIBK, and with constant agitation, the resultant solution was transferred to a round-bottom flask to react at a temperature of 75 °*C* for 3 hours. Thin-layer chromatography (TLC) was performed as the reaction progressed. The films were delicately spread or placed onto a silicon mould after the reactions were complete and then left to dry at room temperature, delicately detached from the mould, and subsequently labelled as CSO-PU, CSO-PU-BPA, and CSO-PU-BPA-MS (0.1 wt%), CSO-PU-BPA-MS (0.3 wt%), CSO-PU-BPA-MS (0.5 wt%), CSO-PU-BPA-MS (1.0 wt%), CSO-PU-BPA-MS (5.0 wt%).

Characterization

The techniques employed to evaluate the physicochemical characteristics of the oil were modified from previously published studies conducted by Akpan et al and Olowokere *et al.*[28,29] Nanalysis model X685, manufactured by Nanalysis Corporation in Canada, was used to conduct nuclear magnetic resonance (^{1}H-NMR) studies. A Fourier transform infrared (FTIR) spectrophotometer (CARY 630, Agilent Technologies, USA) was used for structural elucidation. The surfaces were analyzed morphologically using a Hitachi TM 4000PLUS SEM (Japan) for scanning electron microscopy (SEM) imaging. A Simultaneous Thermal Analyzer (STA6000, PerkinElmer, USA) was used to perform thermogravimetric analysis (TGA) in an inert nitrogen environment.

X-ray diffraction (XRD) was also performed using Siemens D5000 XRD equipment. Data generated by Metrohm Autolab's potentiostat/galvanostat (PGSTAT302 N) were used to plot the Tafel graph, which was used to calculate the corrosion rate. The antimicrobial activity was investigated against both Gram-positive and Gram-negative organisms. A goniometer (model-IL4201 DSA, Krüss GmbH) was used to measure the water contact angle. The salt spray test, as per ASTM B 177–94, was conducted using a salt mist chamber. In the specimen chamber, compressed air was used to atomize a 3.5 wt% NaCl solution.

2. Results and Discussion

2.1. Extraction of Oil

Using a Soxhlet extractor and n-hexane as the solvent, the oil from the castor seed was extracted using a solvent extraction method. A rotary evaporator was used to recover the solvent and concentrate the oil. After being appropriately labelled, the concentrated vegetable oil was kept at room temperature. The extracted castor seed oil (CSO) has a clear golden-yellowish colour and is a free-flowing, slightly viscous liquid at room temperature. The physicochemical properties depend on the substance's chemical and physical attributes. There are standards against which the extracted CSO can be measured. Some of the properties that were examined and listed in Table 1 are the saponification value, specific gravity, iodine value, acid value, viscosity, and refractive index.[28–30]

Table 1. Physicochemical characteristics of CSO.

Properties	CSO
Iodine value (gI_2/100 g)	82.1281
Acid value (mg KOH/g)	3.8831
Specific gravity	0.9583
Viscosity (40 °*C*)	673.05
Free Fatty Acid Value (%)	1.9415
Saponification Value (mg KOH/g)	188.3
Moisture content (%)	5.2
Refractive index (40 °*C*)	1.4765

© 2024 Wiley-VCH GmbH

23656549, 2024, 36, Downloaded from https://chemistry-europe.onlinelibrary.wiley.com/doi/10.1002/slct.202402216 by <Shibboleth>-member@leeds.ac.uk, Wiley Online Library on [24/09/2024]. See the Terms and Conditions (https://onlinelibrary.wiley.com/terms-and-conditions) on Wiley Online Library for rules of use; OA articles are governed by the applicable Creative Commons License

As shown in Figure 4 and Table 2, the FTIR spectrum of the oil showed an absorption band at 857 cm^{-1} for =C–H and a stretching frequency for C–O at 1162 cm^{-1}. The alkane bending frequency for C–H (CH_3) was observed at 1379 cm^{-1}. A peak corresponding to C–H appeared at 1461 cm^{-1}. The non-conjugated alkene C=C stretching bands were observed at 1651 cm^{-1}. The stretching frequency of ester C=O appeared at 1744 cm^{-1}. Symmetric and asymmetric C–H (CH_2) stretching bands appeared at 2855 cm^{-1} and 2925 cm^{-1}, respectively. The absorption band at 3384 cm^{-1} signifies the hydroxyl group attached to the triglycerides of the seed oil.[11]

Table 2. FTIR peaks and corresponding functional groups in CSO.

Peak (cm^{-1})	Type of vibration	Functional group
857	Bending	=C–H
1162	Stretching frequency of ester	C–O
1379	Alkane bending frequency	C–H (CH_3)
1461	Alkane bending	C–H
1651	Non-conjugated alkene stretching	C=C
1744	Stretching frequency of ester	C=O
2855	Symmetric stretching frequency of alkane	C–H (CH_2)
2925	Asymmetric stretching frequency of alkane	C–H (CH_2)
3384	The hydroxyl group of the triglyceride	O–H

2.2. Synthesis of Hybrid Polyurethane (PU)

APTMS (3-aminopropyltrimethoxysilane) was used to modify the silica surface. This process produced free amine (–NH_2) groups on the surface (Figure 2). Thus, modifying the surface characteristics of silica and making it more suitable as a platform for functionalisation.

The backbone of the polyurethane moiety was developed using castor seed oil (CSO) and isophorone diisocyanate (IPDI) to produce pristine PU. This process involves a reaction between the OH group of CSO and the NCO group of IPDI (Figure 1). As represented in Figure 3, the hybrid system was synthesised by impregnating the polymer matrix with 5 wt % bisphenol-A (BPA) and varying the percentage weight of APTMS-modified SiO_2 nanoparticles. The percentages used were 0.1 wt. %, 0.3 wt.%, 0.5 wt.%, 1 wt.%, and 5 wt.%. The synthes-

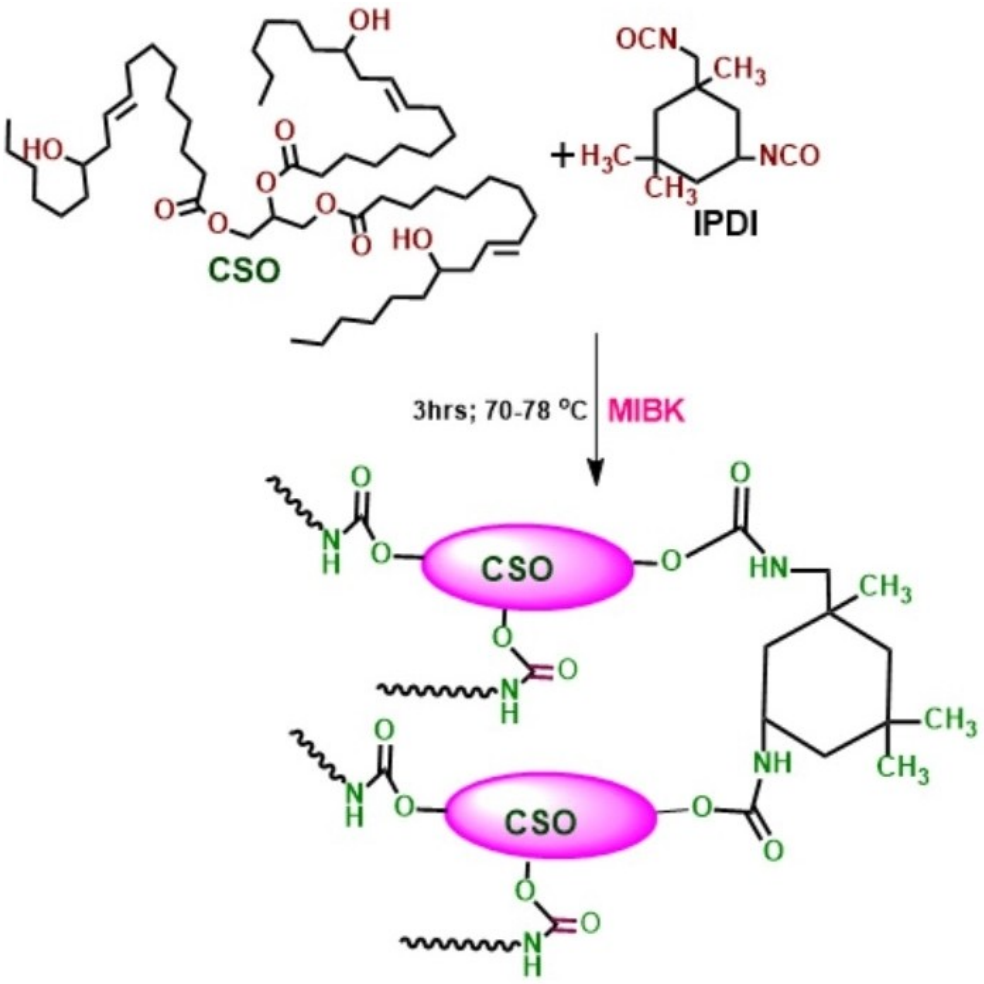


Figure 1. Synthesis of the pristine PU with CSO and IPDI.

© 2024 Wiley-VCH GmbH

23656549, 2024, 36, Downloaded from https://chemistry-europe.onlinelibrary.wiley.com/doi/10.1002/slct.202402216 by <Shibboleth>-member@leeds.ac.uk, Wiley Online Library on [24/09/2024]. See the Terms and Conditions (https://onlinelibrary.wiley.com/terms-and-conditions) on Wiley Online Library for rules of use; OA articles are governed by the applicable Creative Commons License

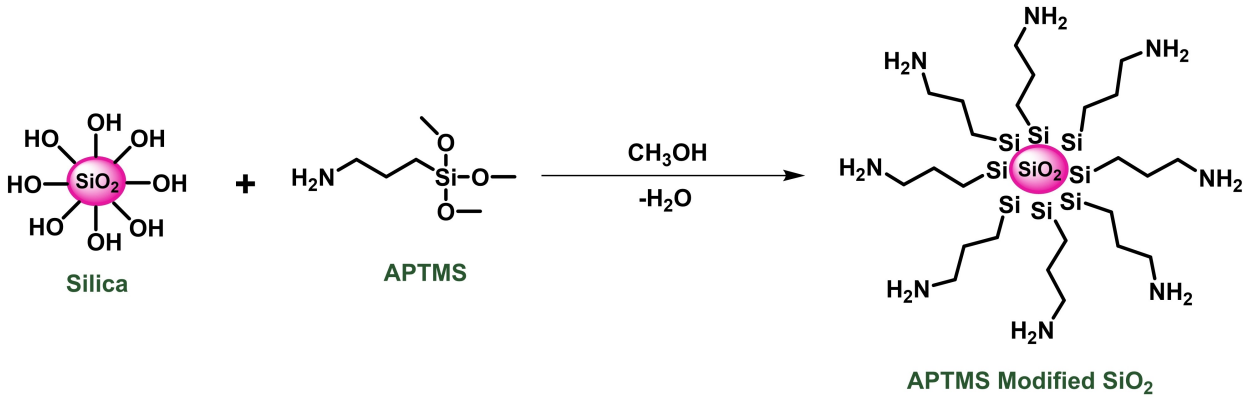


Figure 2. Synthesis of APTMS-modified SiO_2 nanoparticles.

ised films were transparent, soft, and glossy, as shown in Figure 5. The gloss became more pronounced as the percentage of the APTMS-modified SiO_2 nanoparticles increased. Within this polymer, BPA acts as a chain extender, while APTMS-modified SiO_2 functions as the cross-linker.[31–33]

2.2.1. Fourier Transform Infrared

The Fourier transform infrared (FTIR) spectra of all PU polymers in Figure 6 show similar absorption peak characteristics of the various functional groups in a typical polyurethane polymer. Some distinct characteristics are presented in Table 3. Medium alkane CH_2 rocking vibrations were detected at 723 cm^{-1}, indicating the production of polyurethanes. The intensity of this specific peak decreased as the concentration of the silica nanoparticles increased in the polymer matrices from 74.07% in the PU containing 0.1% PU-SNP to 71.305% in 5% PU-SNP. Strong aromatic C–H stretching at 834 cm^{-1} was found in all the samples because they contained BPA, but the intensity decreased from 84.54% in the sample with the lowest content of PU-SNP to 81.25% in the sample with the highest amount of PU-SNP. In addition, at 1640 cm^{-1}, medium aromatic C=C bonds were detected in all films. The decrease in the intensities of these aromatic peaks with an increase in the number of nanomaterials may be attributed to the creation of more cross-linkages within the polymer matrices of the polyurethane moieties. The absorption band at 868 cm^{-1} represents =C–H, while the one at 1028 cm^{-1} represents stretching frequency for C–O in the ester group. C–N stretching occurred at 1304 cm^{-1}, while the alkane bending frequency for C–H in (CH_3) was observed at 1364 cm^{-1}, whereas that of C–H in (CH_2) appeared at 1461 cm^{-1}. The stretching frequencies of ester C=O appeared at 1744 cm^{-1} and 1699 cm^{-1} for the pristine PU but appeared between 1692 cm^{-1} and 1699 cm^{-1} for the hybrid PU with BPA Symmetric and asymmetric C–H (CH_2) stretching bands at

Table 3. FTIR peaks and corresponding functional groups in PU polymers. <

Wavenumber (cm^{-1})	Intensity				
Samples	0.1% PU-SNP	0.3% PU-SNP	0.5% PU-SNP	1% PU-SNP	5% PU-SNP
723	74.07	72.36	73.65	73.71	71.30
834	84.54	82.31	83.90	84.10	81.25
868	87.01	85.19	86.66	87.07	
965		75.61			
1095	ND	57.69	64.89	63.94	
1144	61.99	58.64	61.27	59.91	58.64
1364	76,64	77.96	76.96	77.37	78.30
1461	66.52	68.15	66.90	67.51	68.25
1546	60.54	64.45	62.24	64.77	64.17
1640	66.92	70.75	68.41	71.62	70.18
1699	65.52	64.36	65.00	63.30	65.49
1744				68.66	
2855	71.71	71.48	71.75	70.83	71.96
2925	61.55	61.17	61.54	60.64	61.75
3350	89.37	90.04	89.52	90.34	89.59

© 2024 Wiley-VCH GmbH

23656549, 2024, 36, Downloaded from https://chemistry-europe.onlinelibrary.wiley.com/doi/10.1002/slct.202402216 by <Shibboleth>-member@leeds.ac.uk, Wiley Online Library on [24/09/2024]. See the Terms and Conditions (https://onlinelibrary.wiley.com/terms-and-conditions) on Wiley Online Library for rules of use; OA articles are governed by the applicable Creative Commons License

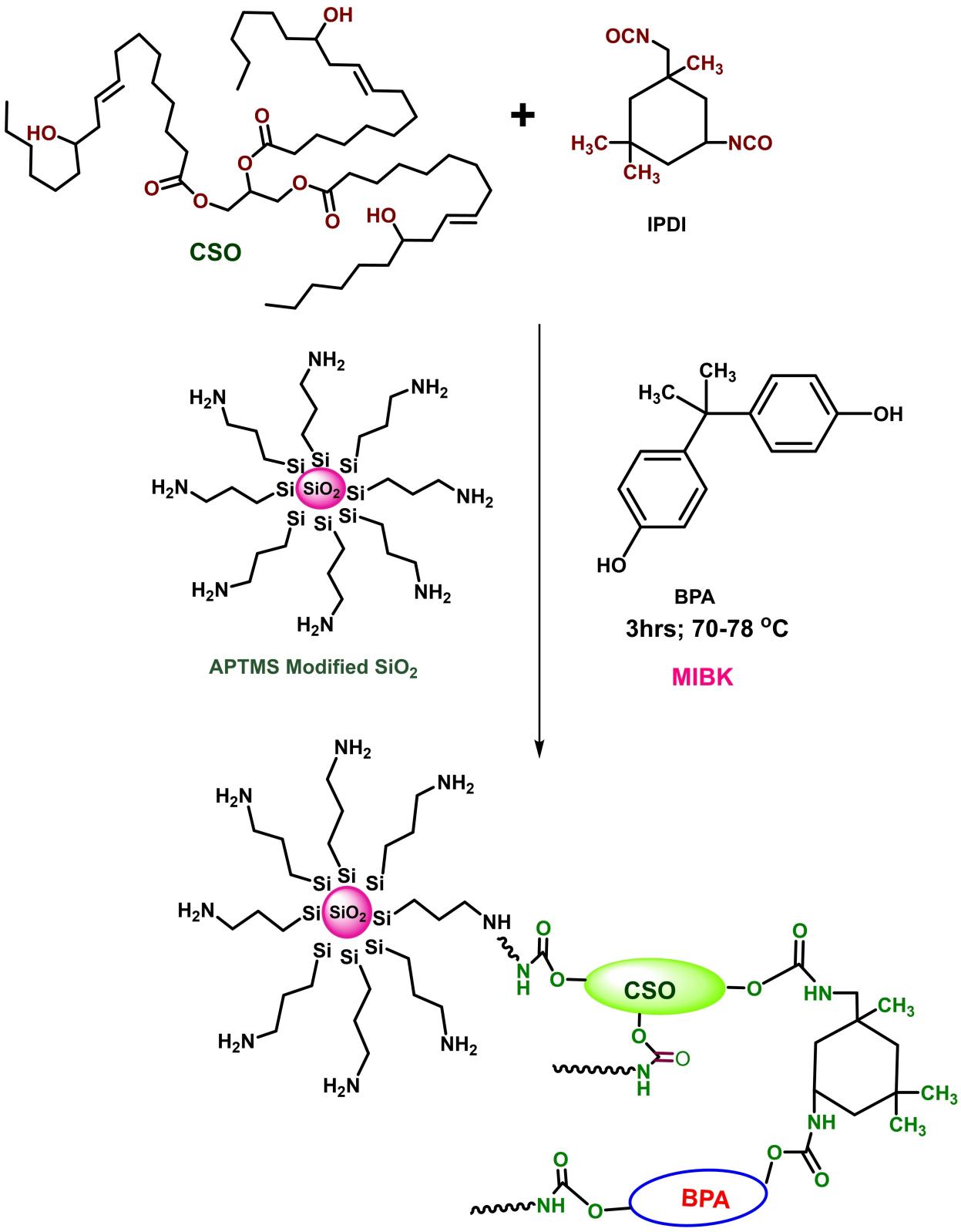


Figure 3. Scheme showing the synthesis of hybrid polyurethane.

2855 cm^{-1} and 2925 cm^{-1}, respectively. The absorption band at 3354 cm^{-1} signifies–NH stretching from the urethane group stretching vibrations. There is no absorption peak observed in the range of 2260 cm^{-1}–2310 cm^{-1}, suggesting that the urethane reaction has reached completion and that the urethane films were completely cured under ambient conditions, hence,

© 2024 Wiley-VCH GmbH

23656549, 2024, 36, Downloaded from https://chemistry-europe.onlinelibrary.wiley.com/doi/10.1002/slct.202402216 by <Shibboleth>-member@leeds.ac.uk, Wiley Online Library on [24/09/2024]. See the Terms and Conditions (https://onlinelibrary.wiley.com/terms-and-conditions) on Wiley Online Library for rules of use; OA articles are governed by the applicable Creative Commons License

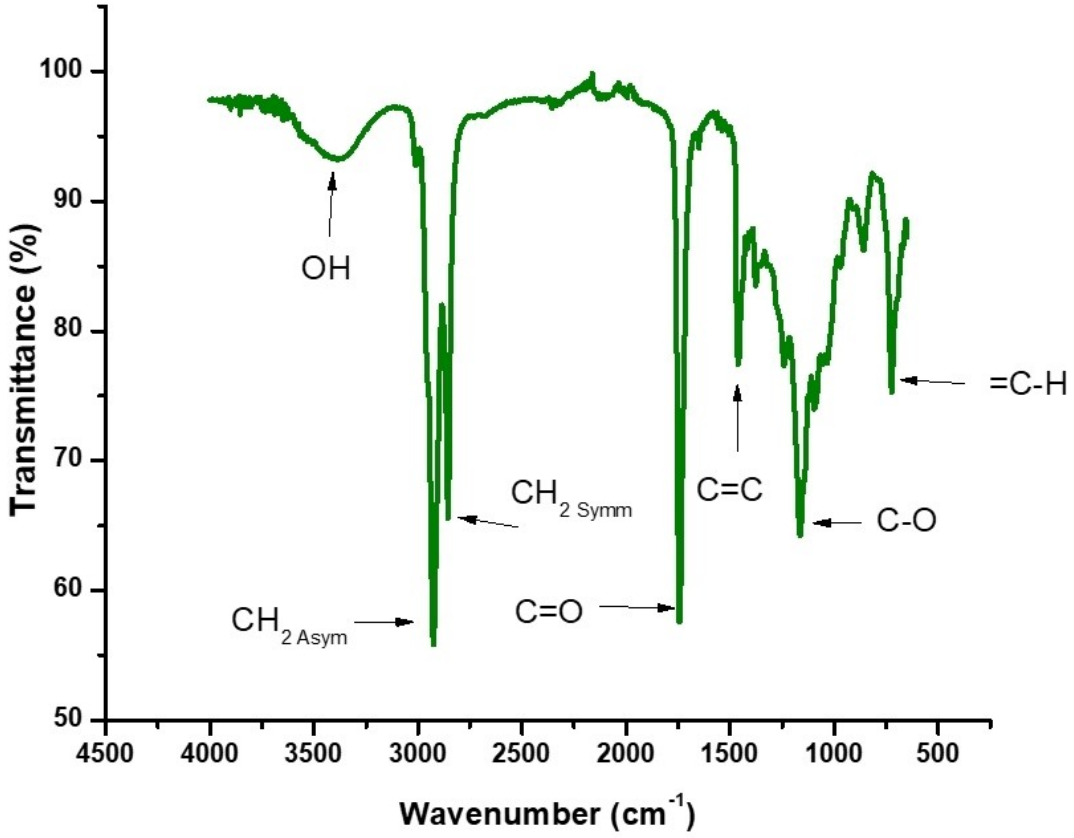


Figure 4. FTIR Spectrum of CSO.



Figure 5. Picture of films where A is the 0.1 wt.% PU-SNP, B is 0.3 wt.% PU-SNP, C is 0.5 wt.% PU-SNP, D is 1 wt.% PU-SNP and E is 5 wt.% PU-SNP.

© 2024 Wiley-VCH GmbH

23656549, 2024, 36, Downloaded from https://chemistry-europe.onlinelibrary.wiley.com/doi/10.1002/slct.202402216 by <Shibboleth>-member@leeds.ac.uk, Wiley Online Library on [24/09/2024]. See the Terms and Conditions (https://onlinelibrary.wiley.com/terms-and-conditions) on Wiley Online Library for rules of use; OA articles are governed by the applicable Creative Commons License

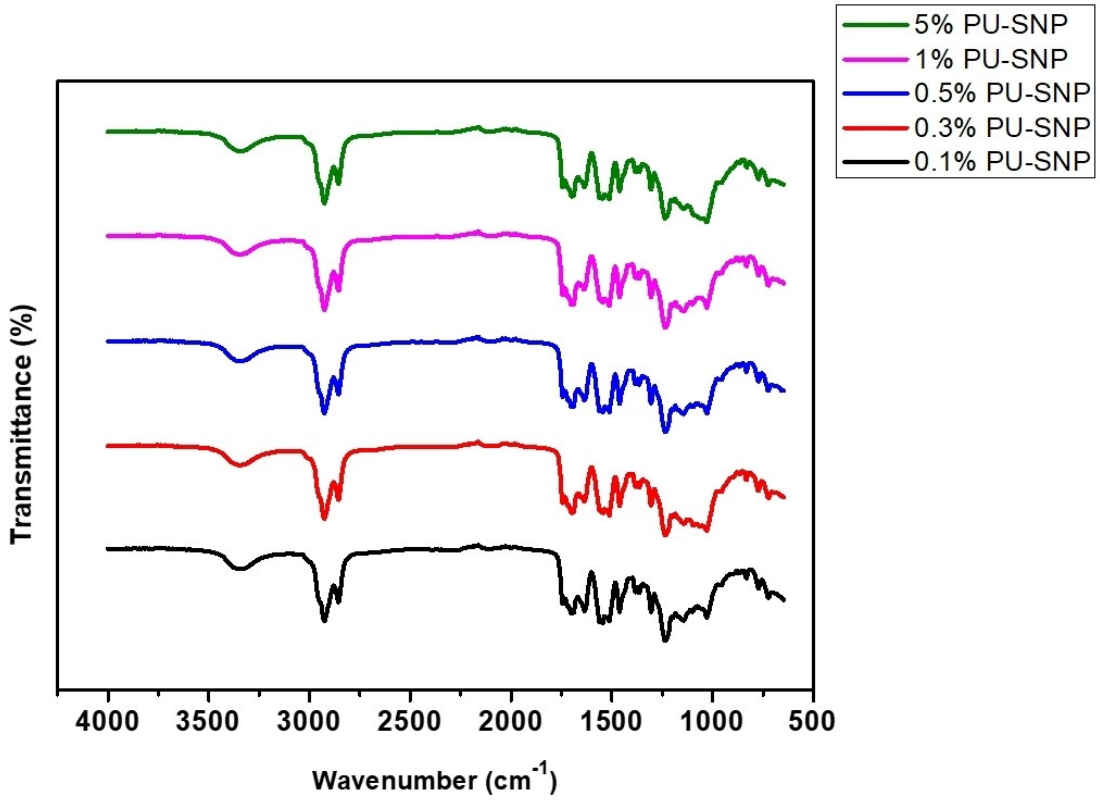


Figure 6. FTIR spectra of the PU-SNP films.

no evidence of any free NCO group in the polymer composition.[11] The peaks corresponding to symmetrical and asymmetrical Si-O–Si stretching vibrations appeared at 834 cm^{-1} and 1095 cm^{-1} respectively, while the Si-OH bending vibration appeared at 965 cm^{-1}.[34]

2.2.2. Mechanical Properties: Thermogravimetric Analysis and Differential Thermogravimetric Analysis

The specimens were heated gradually from the starting ambient temperature to 800 °*C*, at a heating rate of 10 °*C*/min in an inert argon environment. Throughout the heating process, a gas flow rate of 20 cm^3/min was maintained. Analyses using TGA and DTG both showed that the polymer films broke down in three distinct phases, as depicted in Figures 7 and 8. The spectral analysis indicated that trapped solvents and water molecules within the material were released at temperatures ranging from 98 °*C* to 130 °*C*. Hydrocarbon residues were emitted at temperatures ranging from 525 °*C* to 648 °*C*. The first phase of heat degradation involves the disintegration of the urethane linkages. This early stage of breakdown is most likely caused by the separation of the isocyanate and alcohol. The second phase of breakdown can be ascribed to the dissociation of ester bonds, whereas the liberation of hydrocarbon residues is likely the third step. The DTG thermogram's negative gradient slope indicates that the reactions leading to the degradation were endothermic. This discovery is consistent with what has been previously reported.[35]

2.2.3. Morphological Analyses

The scanning electron microscopy (SEM) micrographs in Figure 9 show that A, B, C, D, and E are PU-SNP with 0.1 %, 0.3 %, 0.5 %, 1 %, and 5 % APTMS-modified SiO_2, respectively. Adding APTMS-modified SiO_2 to the polyurethane films made the dispersion of the material more uniform or homogeneous throughout the film. There was a significant reduction in aggregation as the concentration of APTMS-modified SiO_2 increased. Scanning electron microscopy (SEM) revealed surface smoothness, which suggests uniformity in the formation of the coating structure.

A broad peak was observed at approximately $2\theta = 18.79°$ in Figure 10 for all the polymers, which confirms the composite polymers' amorphous microcrystalline nature. The spectra confirmed that the synthesized polymers had a consistent amorphous microcrystalline structure.

2.2.4. Electrochemical Test

Figure 11 shows the Tafel plot, which assesses the electrochemical characteristics of the coatings. The overall corrosion reaction is the sum of cathodic and anodic partial reactions. The

© 2024 Wiley-VCH GmbH

23656549, 2024, 36, Downloaded from https://chemistry-europe.onlinelibrary.wiley.com/doi/10.1002/slct.202402216 by <Shibboleth>-member@leeds.ac.uk, Wiley Online Library on [24/09/2024]. See the Terms and Conditions (https://onlinelibrary.wiley.com/terms-and-conditions) on Wiley Online Library for rules of use; OA articles are governed by the applicable Creative Commons License

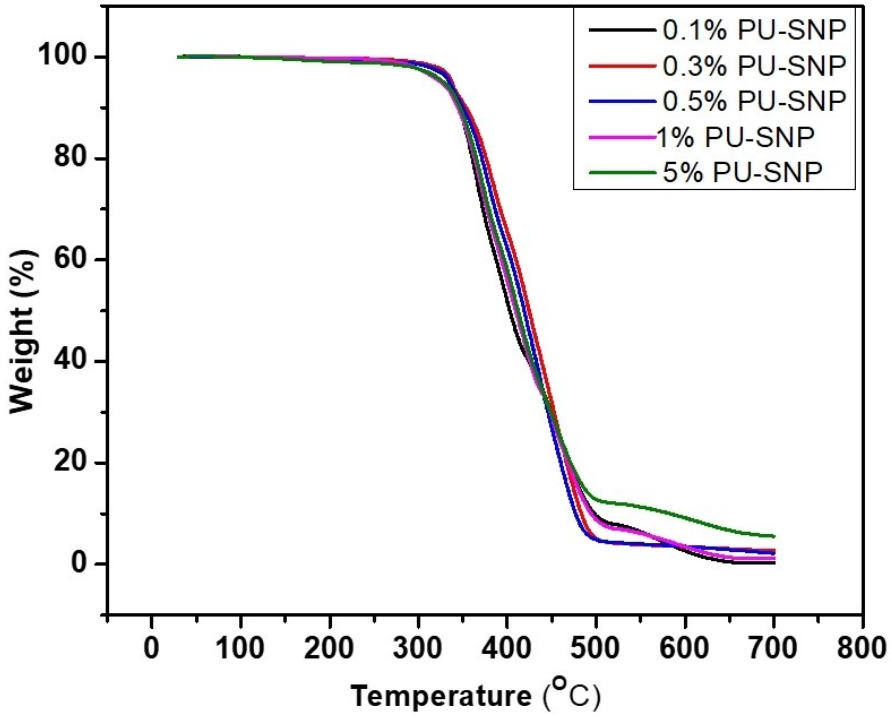


Figure 7. TGA Thermogramms of PU-SNP films.

Tafel equation relates the overpotential of the electrode to the current density passing through it, providing insights into the reaction mechanism. The flow of electrons between anodic and cathodic sites forms the corrosion current, driven by the potential difference between them. Applying polyurethane coatings to the mild steel surfaces caused significant movement of the anodic and cathodic branches towards lower current densities. The observed decrease in the current density suggests the prevention of corrosion. According to Table 4, there is a clear correlation between the polarisation resistance and corrosion rate, showing an inverse relationship. It was observed that the corrosion rate decreased from 0.12362 mm/year for the blank uncoated steel to 0.015077 mm/year for the steel that was coated with 0.1% APTMS-modified SiO_2. An increase in the amount of APTMS-modified SiO_2 impregnated into the polymer saw a further decrease in the corrosion rated to 8.28×10^5 for the steel coated with 5% APTMS-modified SiO_2. E_{corr} and I_{corr} are valuable tools for evaluating and comparing the corrosion resistance of coated materials. A higher E_{corr} number indicates greater corrosion resistance, while a lower I_{corr} value suggests stronger corrosion resistance. The values for both E_{corr} and I_{corr} confirmed that corrosion inhibition increased in the PU-SNP matrix as the proportion of APTMS-modified SiO_2 in the PU matrix increased.

2.2.5. Water Contact Angle

The water contact angle measurements shown in Figure 12 provide additional evidence that the inclusion of APTMS-modified SiO_2 in the polymer matrix affects the water-repellent properties of the coatings. The water contact angle increased with an increase in the amount of the APTMS-modified SiO_2 in the coating system; from 70° for the sample with 0.1% APTM-modified SiO_2 to 84.2° for the sample with 5% APTM-modified SiO_2. The corrosion resistance of polymers is directly proportional to the amount of APTMS-modified SiO_2 present in the

Table 4. Corrosion rates of PU-SNP coatings.

Samples	Corrosion rate(mm/year) R_{corr}	Polarization Resistance ($K\Omega cm^{-2}$)	E_{corr} (mV)	I_{corr} (A/cm^2)
Blank (Uncoated)	0.12362	1.40×10^3	−0.57659	1.06×10^{-5}
0.1% PU-SNP	0.015077	1.49×10^4	−0.5087	1.30×10^{-6}
0.3% PU-SNP	0.00014037	2.54×10^6	−0.33621	1.21×10^{-8}
0.5% PU-SNP	0.00097936	3.13×10^5	−0.50674	8.43×10^{-8}
1% PU-SNP	0.0015561	1.65×10^5	−0.50062	1.34×10^{-7}
5% PU-SNP	8.28×10^5	2.56×10^6	−0.24562	7.13×10^{-9}

© 2024 Wiley-VCH GmbH

23656549, 2024, 36, Downloaded from https://chemistry-europe.onlinelibrary.wiley.com/doi/10.1002/slct.202402216 by <Shibboleth>-member@leeds.ac.uk, Wiley Online Library on [24/09/2024]. See the Terms and Conditions (https://onlinelibrary.wiley.com/terms-and-conditions) on Wiley Online Library for rules of use; OA articles are governed by the applicable Creative Commons License

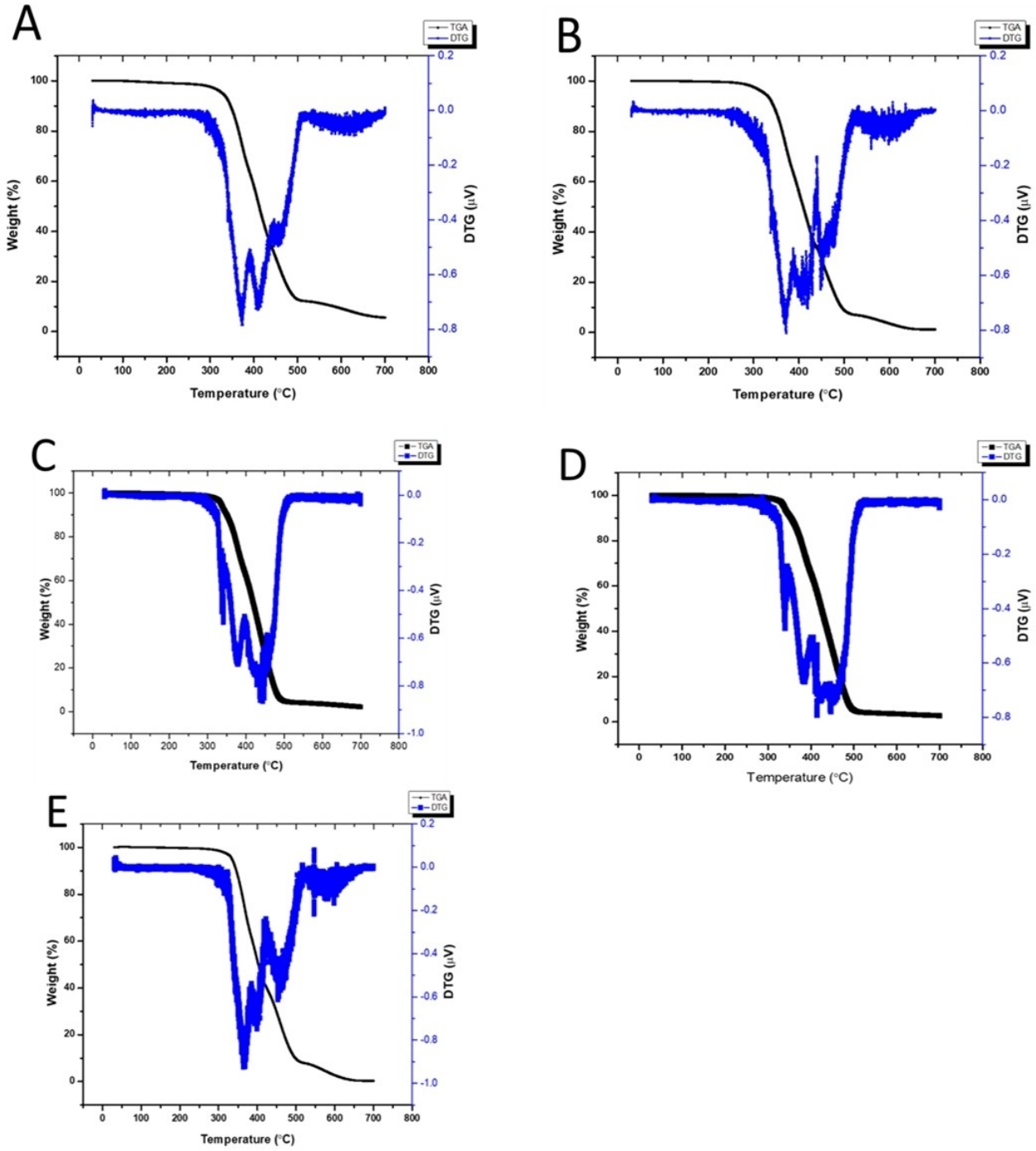


Figure 8. Combined TGA & DTG for A = 0.1 % PU-SNP, B = 0.3 % PU-SNP, C = 0.5 % PU-SNP, D = 1 % PU-SNP, and E = 5 % PU-SNP.

coatings, meaning that polymers containing higher percentages of APTMS-modified SiO_2 exhibit superior corrosion resistance.

2.2.6. Drying Behaviour and Salt Spray Evaluation

Table 5 provides a summary of the drying time and chemical resistance when the PU hybrid resin (PU-SNP) was applied to glass plates. The doped polymeric composite coatings were then rapidly dried. The coatings' drying rate on mild steel can be attributed to the development of highly compact and tightly connected cross-linkages within the polymer matrices.[36] The coated glass plates were submerged in beakers containing different chemical media, as listed in Table 5, at room temperature. Most of the glass plates were stable in water and ethanol. However, the plates soaked in the 5 % NaOH solution exhibited a minor loss of gloss. This observation may be attributed to the presence of an alkali-hydrolyzable ester moiety. Figure 13 is the result of keeping the coated mild steel panels in the salt spray chamber for 720 hours while fog-spraying with a 3.5 % NaCl

© 2024 Wiley-VCH GmbH

23656549, 2024, 36, Downloaded from https://chemistry-europe.onlinelibrary.wiley.com/doi/10.1002/slct.202402216 by <Shibboleth>-member@leeds.ac.uk, Wiley Online Library on [24/09/2024]. See the Terms and Conditions (https://onlinelibrary.wiley.com/terms-and-conditions) on Wiley Online Library for rules of use; OA articles are governed by the applicable Creative Commons License

Research Article
doi.org/10.1002/slct.202402216
Chemistry Europe
European Chemical Societies Publishing

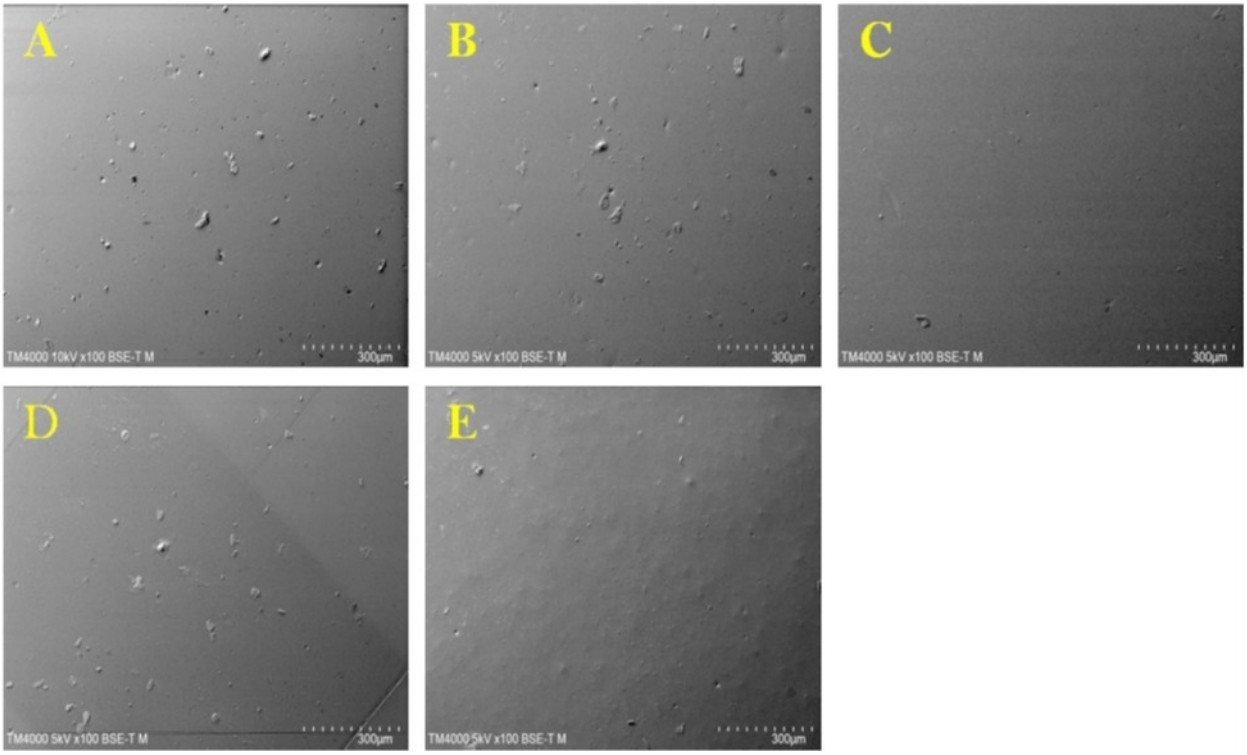


Figure 9. SEM microgrammes of (A) 0.1 %, (B) 0.3 %, (C) 0.5 %, (D) 1 % & (E) 5 % PU-SNP.

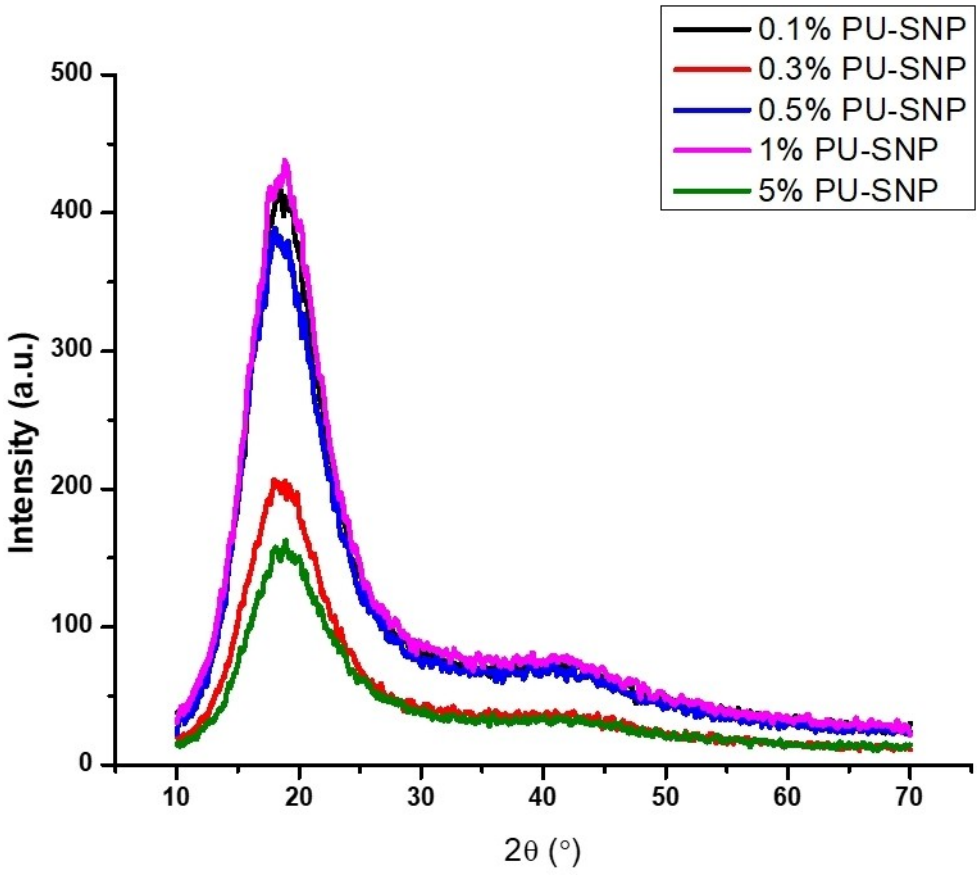


Figure 10. Combined XRD Spectra for PU-SNP hybrid films.

© 2024 Wiley-VCH GmbH

23656549, 2024, 36, Downloaded from https://chemistry-europe.onlinelibrary.wiley.com/doi/10.1002/slct.202402216 by <Shibboleth>-member@leeds.ac.uk, Wiley Online Library on [24/09/2024]. See the Terms and Conditions (https://onlinelibrary.wiley.com/terms-and-conditions) on Wiley Online Library for rules of use; OA articles are governed by the applicable Creative Commons License

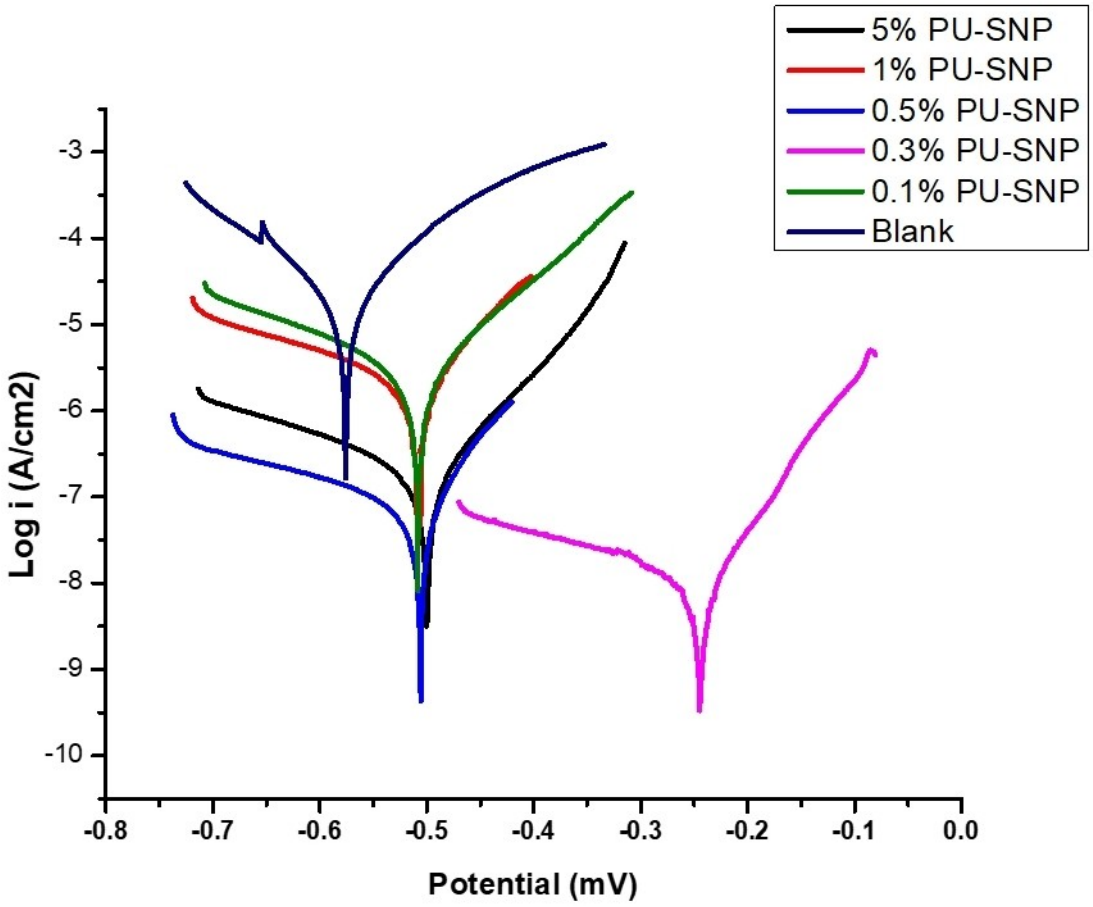


Figure 11. Tafel plots for PU-SNP films.



Figure 12. Water contact angle test.

Table 5. Drying time and Chemical resistance of PU-SNP.

Code	0.1 %PU-SNP	PU-SNP 0.3 %	PU-SNP 0.5 %	PU-SNP 1 %	PU-BPA 5 %
Drying time[a] (day)	3	3	3	2	2
H_2O (10 days)	A	A	A	A	A
EtOH (20 % 7 days)	B	A	A	A	A
NaOH (5 %, 2 h)	C	B	A	A	A
HCl (5 % 10 days)	C	B	B	A	A

A = not affected, B = slightly affected, C = partial delamination of the film, and a = room temperature.

solution. There is more noticeable deterioration on PU-SNP 0.1 wt.% and PU-SNP 0.3 wt.% coated panels, while the PU-SNP 1 wt. % and PU-SNP 5 wt.% coated panels exhibited the highest level of resistance when compared to others. These results suggest that increasing the proportion of modified silica (SiO_2) in the polymer matrices enhances the salt resistance of the coated substrates.

© 2024 Wiley-VCH GmbH

23656549, 2024, 36, Downloaded from https://chemistry-europe.onlinelibrary.wiley.com/doi/10.1002/slct.202402216 by <Shibboleth>-member@leeds.ac.uk, Wiley Online Library on [24/09/2024]. See the Terms and Conditions (https://onlinelibrary.wiley.com/terms-and-conditions) on Wiley Online Library for rules of use; OA articles are governed by the applicable Creative Commons License

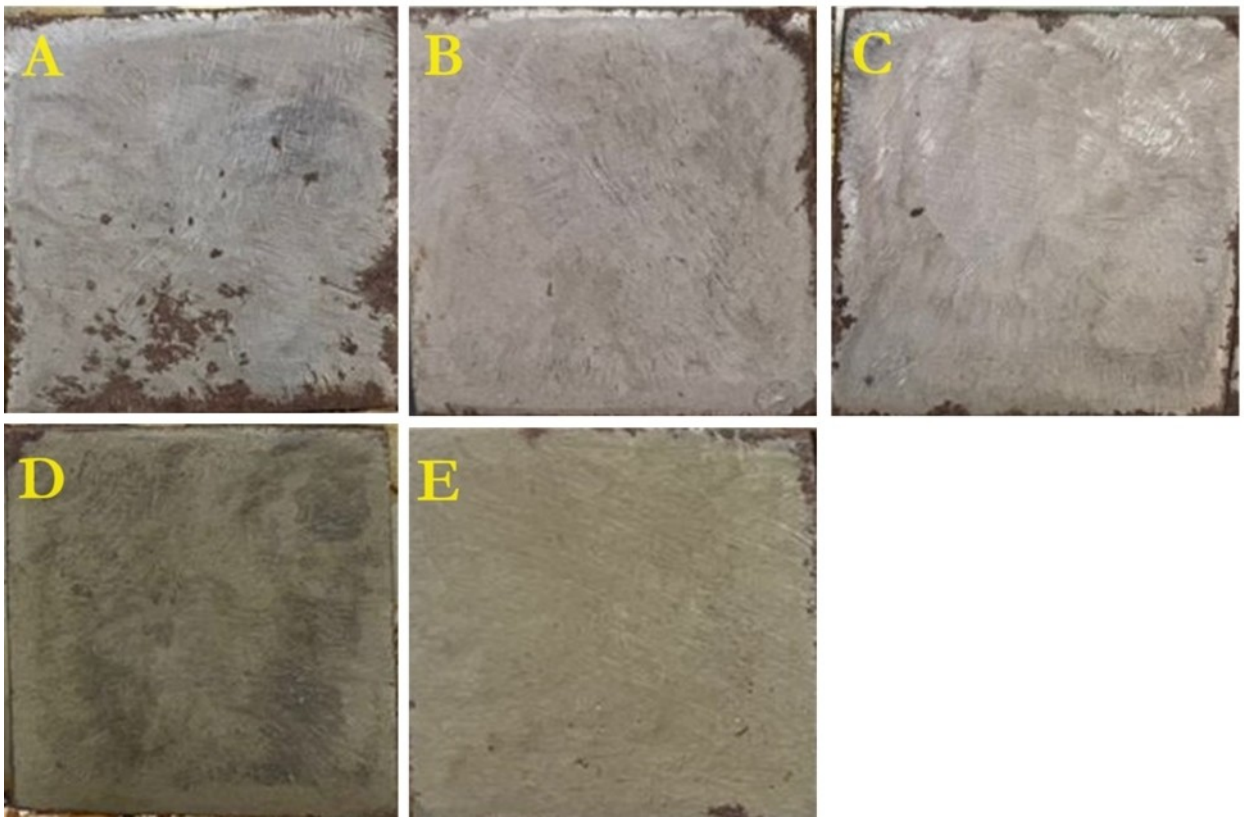


Figure 13. The Salt Spray Test of coatings in 3.5% NaCl solution. Where: (A) 0.1%, (B) 0.3%, (C) 0.5%, (D) 1% & (E) 5% PU-SNP.

2.2.7. Antimicrobial Tests

The antimicrobial activities of the pristine and APTMS-SiO_2 functionalised coating films against tested organisms (*Bacillus subtilis, Aspergillus niger, Escherichia coli, Rhizopus stolonifera, and Staphylococcus aureus*) are presented in Table 6. The coating films with the most percentage composition of modified material (i.e., 5% PU-SNP) showed the best activity against tested organisms. *Bacillus subtilis* was seen to grow overall in test samples, but poor activity was also observed in *Aspergillus niger* with 0.1% PU-SNP and 0.3% PU-SNP.

3. Conclusions

The synthesised composite coatings effectively integrated APTMS-modified SiO_2 nanoparticles into the polymer matrix. These synthetic composites were tested for thermal stability, functional antibacterial efficacy, and corrosion resistance. The hybrid nanoparticles improved the film coating quality for all the parameters investigated. There was no degradation in the photographic view of any of the films tested, even when the percentage of APTMS-modified SiO_2 nanoparticles increased from 0.1 wt% to 5 wt%. Films showed modest activity between 0.5 wt% of APTMS-modified SiO_2 nanoparticles to 5 wt% of APTMS-modified SiO_2 nanoparticles, but *Bacillus subtilis* had no microbial activity.

Table 6. Antimicrobial test results.

Organisms	0.1% PU-SNP	0.3% PU-SNP	0.5% PU-SNP	1%PU-SNP	5%PU-SNP
Bacillus subtilis	−	−	−	−	−
Aspergillus niger	−	−	+	+	+
Escherichia coli	+	+	++	++++	++++
Rhizopus stolonifer	+	++	++	+++	++++
Staphylococcus aureus	+	++	+++	+++	++++

− Inactive, + poorly active, ++ Mildly active, +++ Fairly active, ++++ Moderately active.

© 2024 Wiley-VCH GmbH

23656549, 2024, 36, Downloaded from https://chemistry-europe.onlinelibrary.wiley.com/doi/10.1002/slct.202402216 by <Shibboleth>-member@leeds.ac.uk, Wiley Online Library on [24/09/2024]. See the Terms and Conditions (https://onlinelibrary.wiley.com/terms-and-conditions) on Wiley Online Library for rules of use; OA articles are governed by the applicable Creative Commons License

Acknowledgements

The corresponding author, Dr Tolutope Oluwasegun Siyanbola, appreciates the Indian Institute of Chemical Technology (IICT) and Covenant University for providing the research platform. Special appreciation to Jeff Lawrence, Senior Technician (Materials) at Teesside University, Middlesbrough, (United Kingdom), for his invaluable assistance in instrumentation/data analyses.

Conflict of Interests

The authors declare no conflict of interest. The authors whose names are listed immediately below certify that they have NO affiliations with or involvement in any organization or entity with any financial interest (such as honoraria; educational grants; participation in speakers' bureaus; membership, employment, consultancies, stock ownership, or other equity interest; and expert testimony or patent-licensing arrangements), or non-financial interest (such as personal or professional relationships, affiliations, knowledge or beliefs) in the subject matter or materials discussed in this manuscript.

Data Availability Statement

The data that support the findings of this study are available on request from the corresponding author. The data are not publicly available due to privacy or ethical restrictions.

Keywords: Eco-friendly · Nanomaterials · Polyurethane · Corrosion resistance · Antimicrobial

[1] T. O. Siyanbola, K. Sasidhar, B. V. S. K. Rao, Ramanuj Narayan, O. Olaofe, E. T. Akintayo, K. V. S. N. Raju, *J. Am. Oil Chem. Soc* **2015**, *92*, 267–275.
[2] M. S. Mauter, M. Elimelech, *Environ. Sci. Technol* **2008**, *42*, 5843–5859.
[3] R. Lambourne and T. A. Strivens, Woodhead Pub. Ltd. **1999**.
[4] S. A. Adeboye, A. D. Adebowale, T. O. Siyanbola, K. O. Ajanaku, *IOP Conf. Ser. Earth Environ. Sci.* **2023**.
[5] M. Fernández-Garcia, J. A. Rodriguez, Brookhaven National Laboratory, New York **2007**.
[6] T. O. Siyanbola, K. Sasidhar, B. Anjaneyulu, K. P. Kumar, B. V. S. K. Rao, R. Narayan, O. Olaofe, E. T. Akintayo, K. V. S. N. Raju, *J. Mater. Sci.* **2013**, *48*, 8215–8227.
[7] A. K. Mishra, R. S. Mishra, R. Narayan, K. V. S. N. Raju, *Prog. Org. Coat.* **2010**, *67*, 405–413.
[8] S. Ghosh, S. K. Goswami, L. J. Mathias, *J. Mater. Chem. A* **2013**, *1*, 6073–6080.
[9] Z. Q. Yu, S. L. You, Z. G. Yang, H. Baier, *Adv. Compos. Mat.* **2011**, *20*, 487–502.
[10] Y. Yang, C. Yi, *J. Mater. Sci.* **2019**, *54*, 9456–9465.
[11] T. O. Siyanbola, et al, *Prog. Org. Coat.* **2019**, *131*, 42–48.
[12] G. Kwiatkowski, F. Jähnig, J. Steinhauser, P. Wespi, M. Ernst, S. Kozerke, *Sci. Rep.* **2017**, *7*, 7946.
[13] M. B. Gongalsky, L. A. Osminkina, A. Pereira, A. A. Manankov, A. A. Fedorenko, A. N. Vasiliev, V. V. Solovyev, A. A. Kudryavtsev, M. Sentis, A. V. Kabashin, *Sci. Rep.* **2016**, *6*, 24732.
[14] Y. Wang, Q. Zhao, N. Han, L. Bai, J. Li, J. Liu, E. Che, L. Hu, Q. Zhang, T. Jiang, *Nanomedicine (Lond)* **2015**, *11*, 313–327.
[15] J. Soleymani, M. Hasanzadeh, M. H. Somi, N. Shadjou, A. Jouyban, *Biosens. Bioelectron.* **2018**, *115*, 61–69.
[16] G. Kwiatkowski, F. Jähnig, J. Steinhauser, P. Wespi, M. Ernst, S. Kozerke, *Sci. Rep.* **2017**, *7*, 7946.
[17] Y. Fan, A. Girard, M. Waals, C. Salzemann, A. Courty, *ACS Appl. Nano Mater.* **2023**, *6*, 1193.
[18] M. Ghodrati, M. Mousavi-Kamazani, Z. Bahrami, *Sci. Rep.* **2023**, *13*, 548.
[19] A. Liberman, N. Mendez, W. C. Trogler, A. C. Kummel, *Surf. Sci. Rep.* **2014**, *69*, 132.
[20] J. G. Croissant, K. S. Butler, J. I. Zink, C. F. Brinker, *Nat. Rev. Mater.* **2020**, *5*, 886.
[21] P. Singh, S. Srivastava, S. K. Singh, *ACS Biomater. Sci. Eng.* **2019**, *5*, 4882.
[22] A. A. Nayl, A. I. Abd-Elhamid, A. A. Aly, S. Brase, *RSC Adv.* **2022**, *12*, 13706.
[23] E. Bagheri, L. Ansari, K. Abnous, S. M. Taghdisi, F. Charbgoo, M. Ramezani, M. Alibolandi, *JCR* **2018**, *277*, 57.
[24] C. I. C. Crucho, *Compounds* **2023**, *3*, 280.
[25] T. O. Siyanbola, et al, *Prog. Org. Coat.* **2021**, *161*, 106469.
[26] M. A. R. Meier, J. O. Metzgerb, U. S. Schubert, *Chem. Soc. Rev.* **2007**, *36*, 1788–1802.
[27] E. Sharmin, S. M. Ashraf, S. Ahmad, *Eur. J. Lipid Sci. Tech.* **2007**, *109*, 134–146.
[28] J. A. Olowokere, A. I. Onen, M. C. Odineze, I. D. B'aga, and J. N. Akoji, *Asian J. Appl. Chem. Res.* **2019**, 1–11.
[29] U. G. Akpan, A. Jimoh, A. D. Mohammed, *Leonardo J. Sci.* **2006**, *8*, 43–52.
[30] J. K. C. Nduka, P. O. Omozuwa, and O. E. Imanah, *Arabian J. Chem.* **2021**, 14.
[31] M. Joo, T. M. Chiu, H. Castaneda, M. D. Soucek, *Prog. Org. Coat.* **2019**, *134*, 209–218.
[32] M. Choi, W. K. Choi, C. H. Jung, and S. B. Kim, *Sci. Rep.* **2020**, 10.
[33] L. Meng, H. Zhu, B. Feng, Z. Gao, D. Wang, and S. Wei, *Prog. Org. Coat.* **2020**, 141.
[34] A. Kawsihan, et al., *RSC Adv.* **2023**, *13*, 28852–28860.
[35] T. O. Siyanbola et al., *Sci. African* **2023**, 20.
[36] S. Adeboye, et al., *Ind. Crops Prod.* **2024**, *214*, 118475.

Manuscript received: May 8, 2024

© 2024 Wiley-VCH GmbH

23656549, 2024, 36, Downloaded from https://chemistry-europe.onlinelibrary.wiley.com/doi/10.1002/slct.202402216 by <Shibboleth>-member@leeds.ac.uk, Wiley Online Library on [24/09/2024]. See the Terms and Conditions (https://onlinelibrary.wiley.com/terms-and-conditions) on Wiley Online Library for rules of use; OA articles are governed by the applicable Creative Commons License